

Article

A Single Eu-Doped In₂O₃ Nanobelt Device for Selective H₂S Detection

Weiwu Chen, Yingkai Liu *, Zhaojun Qin, Yuemei Wu, Shuanghui Li and Peng Ai

Received: 3 October 2015; Accepted: 26 November 2015; Published: 30 November 2015

Academic Editor: Michael Tiemann

Institute of Physics and Electronic Information Technology, Yunnan Normal University, Kunming 650500, China; chenweiwu55@163.com (W.C.); qinzhaojun031@163.com (Z.Q.); wuyuemei893@163.com (Y.W.); lishuanghui808@163.com (S.L.); aipeng114@163.com (P.A.)

* Correspondence: ykliu@ynnu.edu.cn; Tel.: +86-871-6591-1286; Fax: +86-871-6594-1168

Abstract: Eu-doped In₂O₃ nanobelts (Eu-In₂O₃ NBs) and pure In₂O₃ nanobelts (In₂O₃ NBs) are synthesized by the carbon thermal reduction method. Single nanobelt sensors are fabricated via an ion beam deposition system with a mesh-grid mask. The gas-sensing response properties of the Eu-In₂O₃ NB device and its undoped counterpart are investigated with several kinds of gases (including H₂S, CO, NO₂, HCHO, and C₂H₅OH) at different concentrations and different temperatures. It is found that the response of the Eu-In₂O₃ NB device to 100 ppm of H₂S is the best among these gases and the sensitivity reaches 5.74, which is five times that of pure In₂O₃ NB at 260 °C. We also found that the former has an excellent sensitive response and great selectivity to H₂S compared to the latter. Besides, there is a linear relationship between the response and H₂S concentration when its concentration changes from 5 to 100 ppm and from 100 to 1000 ppm. The response/recovery time is quite short and remains stable with an increase of H₂S concentration. These results mean that the doping of Eu can improve the gas-sensing performance of In₂O₃ NB effectually.

Keywords: Eu-doped In₂O₃; single nanobelt; gas sensor; H₂S

1. Introduction

Due to its unique properties and special application prospects, low-dimensional metal-oxide semiconductor nanomaterials have been widely investigated in recent years [1–3]. For instance, Lu *et al.* have reported that Zn₂GeO₄ nanowires are prepared as a photoanode for quantum dot-sensitized solar cells and show an excellent performance [4]. For detecting poisonous or flammable gases, it is necessary to develop one-dimensional nano-scale gas sensors with high selectivity and sensitivity due to their fast response, low power consumption, and long-term reliability [5,6]. Among various active sensing materials, In₂O₃, as an n-type semiconductor with a wide band gap (~2.9 eV) and good chemical and thermal stabilities under practical operating conditions, has been widely used as a gas sensor [7,8]. Sun *et al.* have reported that In₂O₃ with appropriate mesostructured ordering has the potential to detect ethanol [9]. Lai *et al.* have reported that In₂O₃ nanorods have a good response to formaldehyde [10]. These investigations confirm that indium oxide nanomaterials really have good gas-sensitive properties. In order to gain higher response and selectivity, an additional noble metal as catalyst is efficient [11]. The effects of the addition of Au, Ag, La, and Ta on sensitive properties have been reported [12–15]. Shen *et al.* have found that Eu³⁺ can improve the performance of the bio-MOF-1 hybrid system for sensing organic amine vapors [16]. Hao *et al.* have reported that Eu can enhance sensing and electronic conductivity of metal-organic frameworks [17]. However, to the best of our knowledge, attention has been focused on the morphological or optical properties of Eu-doped In₂O₃ nanomaterials instead

of their gas-sensitive properties [18,19]. Meanwhile, several features such as flexible structure, structural homogeneity, and crystallographic perfection make nanobelts a great choice for sensor devices [7]. Li *et al.* have obtained the formaldehyde gas-sensing properties of In_2O_3 nanofibers and nanobelts [20]. Their results showed that the highest response of the In_2O_3 nanobelt sensor ($R_a/R_g = 4.214$ at $300\text{ }^\circ\text{C}$, where R_a is the sensor resistance in the air and R_g is the resistance in the tested gas) is higher than that of the In_2O_3 nanofiber sensor ($R_a/R_g = 3.113$ at $340\text{ }^\circ\text{C}$). In addition, Ma *et al.* have found that the best working temperature of the SnO_2 nanobelt sensor is $230\text{ }^\circ\text{C}$, which is much lower than that of tin dioxide nanoflower and porous nanosphere sensors ($400\text{ }^\circ\text{C}$) reported by Hoa *et al.* [21,22]. The above-mentioned literature revealed that, compared to other nanodevices, nanobelt sensors have unique advantages. Therefore, there is a great demand to study the gas-sensing properties of $\text{Eu-In}_2\text{O}_3$ NBs.

In this paper, we present the synthesis of In_2O_3 NBs and $\text{Eu-In}_2\text{O}_3$ NBs by the carbon thermal reduction method. Then, the sensing properties of a single NB to five kinds of gases are measured. Compared with those of the pure NB, the $\text{Eu-In}_2\text{O}_3$ NB sensor has higher response and better selectivity to H_2S . The $\text{Eu-In}_2\text{O}_3$ NBs show great potential in gas-sensing applications.

2. Experimental Section

The NBs were synthesized by the carbon thermal reduction method in a horizontal alundum tube (outer diameter of 4.0 cm, length of 100 cm) which was mounted inside a high-temperature tube furnace (HTF). For synthesizing $\text{Eu-In}_2\text{O}_3$ NBs, the mixture consists of In_2O_3 , $\text{Eu}(\text{O}_2\text{CCH}_3)_3$, and carbon powders (mass ratio~20:1:10). As for pure In_2O_3 NBs, the mixture is composed of In_2O_3 and carbon powders (mass ratio~2:1). The mixtures were put into a ceramic boat and then the boat was placed at the center of the HTF. A silicon wafer coated with 10-nm-thick Au film was put into the HTF with a distance of ~20 cm from the ceramic boat in the downstream and the tube was cleaned three times by argon gas. Then, the tube was evacuated by a mechanical pump to a pressure of 1–5 Pa. The center temperature of the HTF was increased to $1060\text{ }^\circ\text{C}$ at a ramp rate of $10\text{ }^\circ\text{C}/\text{min}$ and was maintained at this temperature for 120 min. In these processes, argon as a carrier gas was flowed at 20 sccm and oxygen was aerated at 10 sccm when the temperature of the HTF reached $600\text{ }^\circ\text{C}$. During the deposition process we adjusted the suction speed of the mechanical pump to keep the inside pressure 200 Torr. After the HTF was naturally cooled to room temperature, white materials deposited on the substrate were obtained.

The morphology, structure, and composition of the samples were characterized by X-ray diffraction (XRD), scanning electron microscopy (SEM), energy dispersive X-ray spectroscopy (EDS), transmission electron microscopy (TEM), and high resolution transmission electron microscopy (HRTEM).

In order to analyze the sensing performance of a single NB, the fabrication of the single nanobelt device was necessary. The NBs were first scratched by the tweezers and scattered in ethanol. Several drops of the soliquid were dropped onto a p-type silicon substrate with a 500 nm thick SiO_2 layer. After the ethanol evaporated completely, the Si substrate with the desired NB density was put into a mesh-grid mask and was deposited with inerratic Ti (8 nm) and Au (80 nm) electrodes by ion beam deposition. The background vacuum of the device was 1.0×10^{-4} Pa and the vacuum was held at 2.2×10^{-2} Pa during the deposition. In the deposition process, the argon was flowed and the flux was $10\text{ mA}/\text{cm}^2$. The schematic diagram of the prepared device is shown in Figure 1a and the optical microscopic image of a single nanobelt device is displayed in Figure 1b. Figure 1c presents the SEM image of Figure 1b, which is used for all gas-sensing measurements. The length and width of the measured nanobelt are about $12.287\text{ }\mu\text{m}$ and $2.188\text{ }\mu\text{m}$, respectively. It is observed that two ends of the single nanobelt are covered with Ti/Au electrodes on top of it. The measurements were conducted in a hermetic stainless steel vessel (20 L) and the sensor was placed on a temperature control platform. The target liquid or gas would be injected into an evaporator to evaporate rapidly

and the atmosphere in the chamber was made uniform by a fan. Finally, the gas-sensing performance of the prepared devices was measured by Keithley 4200.

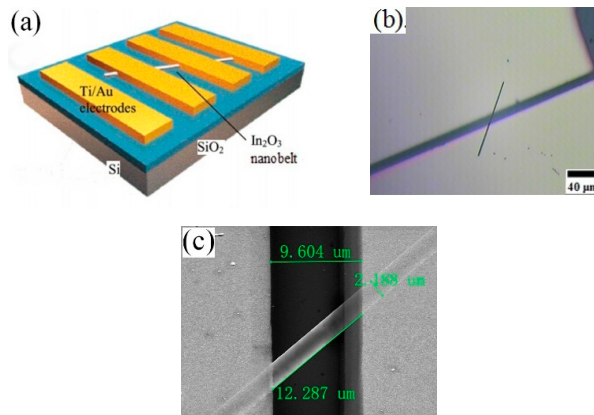


Figure 1. (a) A schematic diagram of the device; (b) The photo of the single nanobelt device; (c) SEM image of a single nanobelt device with Ti/Au electrodes on top of it.

3. Results and Discussion

3.1. Structures

SEM images of Eu-In₂O₃ NBs are presented in Figure 2. It is seen that a large number of NBs were deposited on the substrate in Figure 2a. The length of the obtained NBs reaches several hundred micrometers. Figure 2b is the enlarged image of the local area of Figure 2a and shows that the width with uniform size is about several micrometers. Its surface is smooth and transparent, indicating that the thickness is very thin.

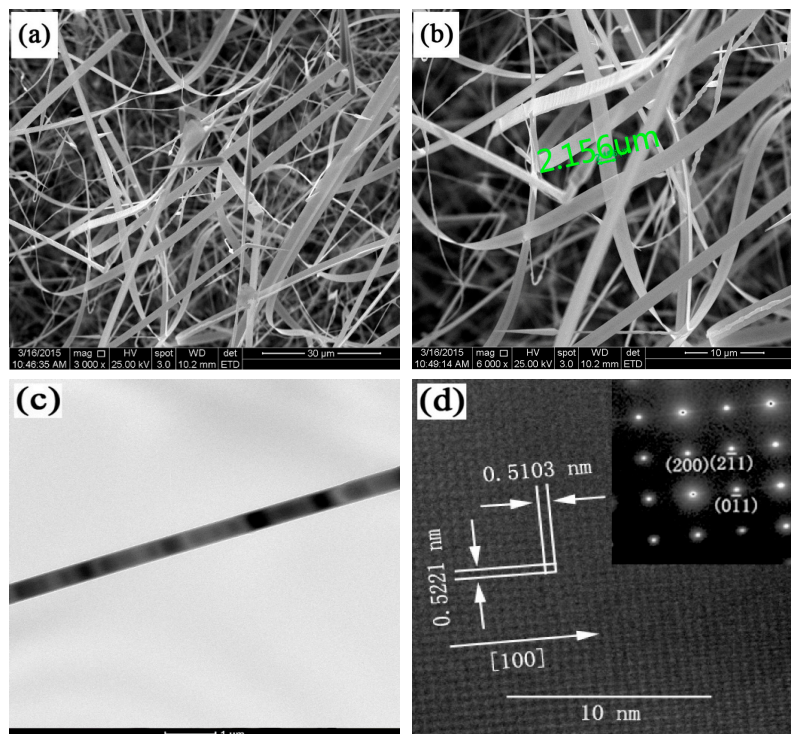


Figure 2. (a) Large-area SEM image; (b) Higher magnification SEM micrograph of Eu-In₂O₃ NBs; (c) TEM image of Eu-In₂O₃ NB; (d) HRTEM image, the inset: SAED pattern.

Figure 2c shows a TEM image of a Eu-In₂O₃ NB. It reveals that its width is about 480 nm. The HRTEM image and SAED pattern are displayed in Figure 2d and its inset. The interplanar spacings are 0.5221 nm and 0.5103 nm, corresponding to the (2 0 0) and (0 -1 1) crystal planes. The SAED pattern is indexed to the cubic In₂O₃ structure with $a = b = c = 1.011$ nm, indicating that it was a single crystal. Comparing HRTEM and SAED images, it is drawn that the growth direction of Eu-In₂O₃ NBs is along [1 0 1] and no obvious structural defects exist.

The XRD patterns of Eu-In₂O₃ and In₂O₃ NBs are displayed in Figure 3a. It shows that all well-defined diffraction peaks can be indexed as the cubic In₂O₃ phase with $a = b = c = 1.011$ nm (JCPDS Card No.06-0416). The prepared sample is well crystallized and no diffraction peaks of other impurities or crystalline by-products are detected. The inset of Figure 3a illustrates that the peak (located at $\sim 30^\circ$) of Eu-In₂O₃ shifts to a lower angle compared with that of In₂O₃ (at 30.6°), indicating that the constants of the latter are larger than those of the former because the radius of Eu ions (94.7 pm) is larger than that of In ions (80 pm). This result reveals that Eu is doped in the lattice. To further make sure whether Eu is doped into the lattices of In₂O₃ or not, an energy-dispersive X-ray spectroscopy (EDS) of Eu-In₂O₃ NBs was carried out, as shown in Figure 3b. It confirms that Eu has been doped into the nanobelts and the content of Eu is 0.86 wt.%. Figure 3c presents I-V curves of the In₂O₃ NB and Eu-In₂O₃ NB. It is noted that the curves are nearly linear, revealing that good ohmic contacts are formed between the Eu-In₂O₃ NB/In₂O₃ NB and the electrodes. Besides, the resistance of the Eu-In₂O₃ NB is lower than that of its pure counterpart, indicating that the dopant improves the conductance of the In₂O₃ NB.

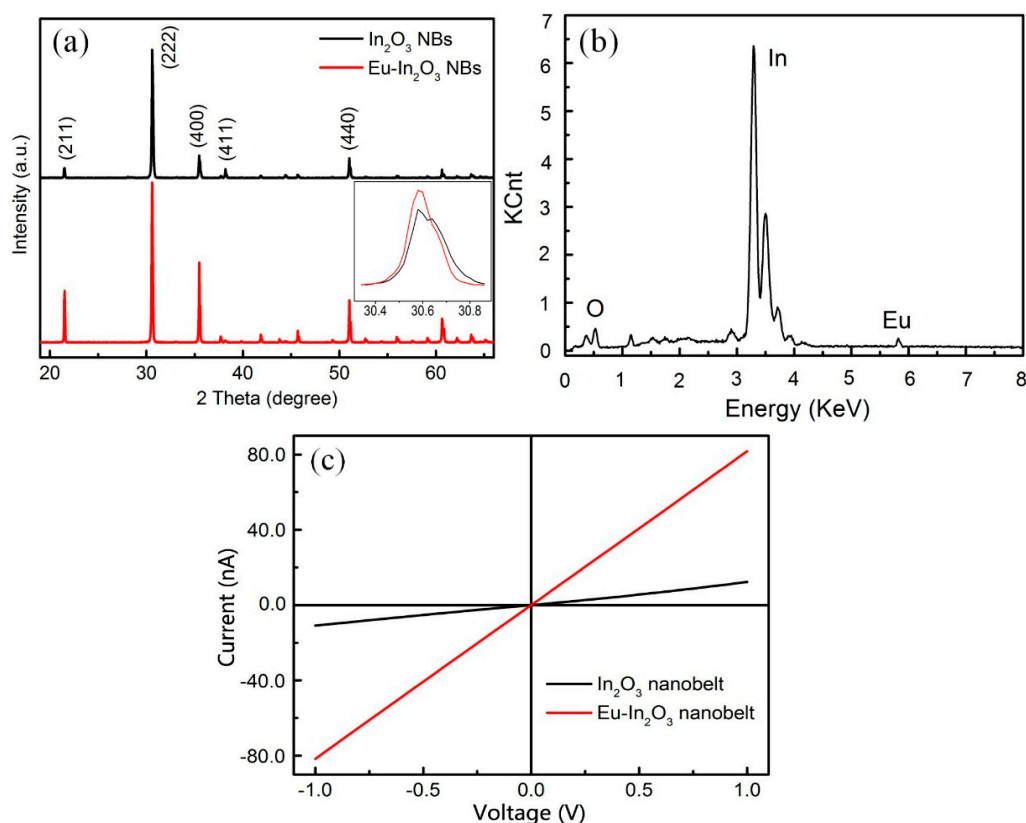


Figure 3. (a) XRD images of Eu-In₂O₃ and In₂O₃ NBs and the inset is the position of the peak at 30.6° ; (b) EDS pattern of Eu-In₂O₃ NBs; (c) The I-V curves of the In₂O₃ NB and Eu-In₂O₃ NB.

3.2. Sensing Properties

The sensitivity is defined as R_a/R_g where R_a is the sensor resistance in the air and R_g is the resistance in the tested gas or R_g/R_a at an oxidizing one. Figure 4a shows the sensitivity curves of

the Eu-In₂O₃ NB and In₂O₃ NB to 100 ppm of H₂S at different temperatures and its inset shows the sensitivity curves of the Eu-In₂O₃ NB to different gases at different temperatures. It is obvious that the optimum operating temperatures of the two devices to five tested gases are 260 °C. Furthermore, the response of the Eu-In₂O₃ device to H₂S reaches 5.74, which is five times that of its pure counterpart. The histogram of two devices corresponding to different gases at 260 °C is shown in Figure 4b. The responses to 100 ppm of CO, NO₂, HCHO, and C₂H₅OH at 260 °C are only 1.31, 1.25, 1.19, and 2.21, respectively. The response to H₂S is several times higher than that of the other four gases, meaning this sensor is more sensitive to hydrogen sulfide. It is noted that the doping of Eu obviously improves the response to H₂S. Although it also increases the responses to other gases, they are not outstanding compared to H₂S.

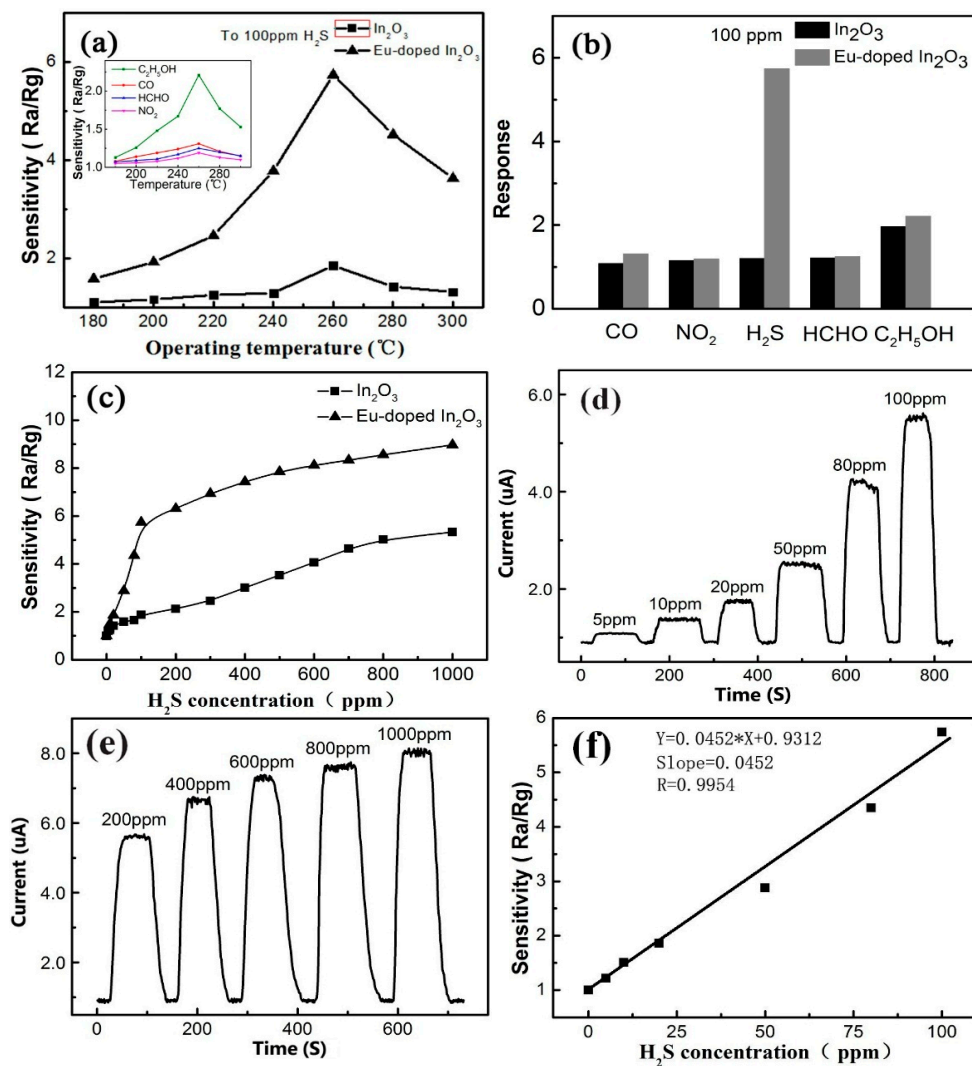


Figure 4. (a) The sensitivity curves of Eu-In₂O₃ NB and In₂O₃ NB to 100 ppm of H₂S at different temperatures and the inset is the sensitivity curves of Eu-In₂O₃ NB to different gases at different temperatures; (b) Histogram of two devices responding to different gases at 260 °C; (c) Response curves of Eu-In₂O₃ NB to H₂S at 5–1000 ppm at 260 °C; (d) Responses curve of Eu-In₂O₃ NB to H₂S at 5–100 ppm at 260 °C; (e) Response curve of Eu-In₂O₃ NB to 200–1000 ppm of H₂S at 260 °C; (f) Fitting the curve of response *versus* H₂S concentration in the range of 5–100 ppm.

The responses to different H₂S concentrations at 260 °C are tested, as shown in Figure 4c. It is seen that there is a linear relationship between the response and H₂S concentrations when the concentration changes from 0 to 100 ppm and from 100 to 1000 ppm. It is noted that the slope of

5 to 100 ppm is higher than that of 100 to 1000 ppm, illustrating that the response increases slowly in this range. The surface coverage tends to saturate and leads to the slope getting smaller at higher concentrations [23] in that the surface coverage of the adsorbed molecules follows the Langmuir isotherm. In our experiment, the minimum detection concentration of the Eu-In₂O₃ sensor is about 5 ppm to H₂S. As reported in the literature, though the minimum detection concentration of In₂O₃ can reach about several hundred ppb to H₂S, the specific surface area of these nanostructures is always much larger [8]. For instance, Zhao *et al.* have reported the lowest detection concentration limit of a In₂O₃ nanotube device could reach 500 ppb for H₂S, but that device is composed of many nanotubes, not a single one [5].

Figure 4d shows the responses curves of Eu-In₂O₃ NB to 5~100 ppm of H₂S at 260 °C and it is seen that six cycles are recorded, corresponding to 5, 10, 20, 50, 80, and 100 ppm of H₂S. It can be seen that the resistance of In₂O₃ NB declines significantly upon injection of H₂S and returns to its original state when H₂S is expelled. Response/recovery time is an important parameter for a gas sensor. For 5~100 ppm of H₂S, the response (recovery) time of the Eu-In₂O₃ NB is 9 (11), 11 (11), 13 (14), 10 (13), 12 (18), and 11 (13) s, respectively. Obviously, the response/recovery time changes little with an increase of H₂S concentration and is less than 18 s, manifesting fast response speed. In addition, the response curves of the Eu-In₂O₃ NB to H₂S at high concentrations at 260 °C are shown in Figure 4e. Repeated measurements have been carried out at each concentration and the results are stable and reliable, indicating that the nanobelt device possesses good repeatability and stability.

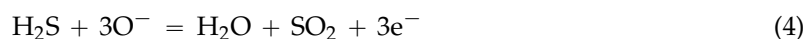
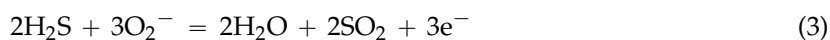
Fitting the curve of response *versus* H₂S concentration in the range of 5–100 ppm is presented in Figure 4f. It can be seen that the slope of the curve is 0.0452 ppm⁻¹ with a fitting quality of R = 0.9954. The sensor noise is calculated by the variation in the relative response in the baseline with help of root-mean-square deviation (RMSD) [24,25]. Then, 120 data points (N) of Figure 4d at the baseline are collected, and the standard deviation (S) is obtained as 0.0932. According to $RMS_{noise} = \sqrt{S^2/N}$, RMS_{noise} is 0.0085 for the H₂S sensor. The theoretical detection limit of the sensor is 0.564 ppm based on the signal-to-noise ratio using DL (ppm) = 3 × (RMS_{noise}/Slope).

3.3. Sensing Mechanism

In₂O₃ is an n-type semiconductor and free electrons are major charge carriers [26]. The In₂O₃ NB adsorbs oxygen-negative ions (O²⁻, and O⁻) resulting from a combination of oxygen molecules and electrons by Equations (1) and (2), which makes the electrical conductivity of In₂O₃ NB reduce [27,28].



The following reactions will occur on the surface of it when In₂O₃ NB is in the strong reducing atmosphere of H₂S.



According to these reactions, the electrons are released, and the conductivity of the nanobelt is enhanced. On one hand, rare earth ions can promote these reactions as a catalyst, leading to the improvement of the sensitivity [29]. On the other hand, the doping of Eu can effectively increase the number of oxygen vacancies because In₂O₃ NBs belong to an n-type semiconductor and oxygen vacancies usually provide donor states [30,31]. Thus, the electric conductivity of In₂O₃ NBs enhances.

4. Conclusions

Eu-doped In₂O₃ NBs and pure In₂O₃ NBs have been prepared by the carbon thermal reduction method. The sensitive properties of two devices based on a single Eu-In₂O₃ NB and its undoped

counterpart have been measured using various gases at different concentrations and temperatures. It is found that the response of the Eu-In₂O₃ device to 100 ppm H₂S reaches 5.74, which is fivetimes that of its undoped counterpart, at 260 °C. A linear relationship between the response and different H₂S concentrations is obtained when the concentration changes from 5 to 100 ppm and from 100 to 1000 ppm. The theoretical detection limit of the Eu-doped In₂O₃ NB sensor is 0.564 ppm at optimum working temperature. It reveals that the doping of Eu improves the sensing performance of In₂O₃ NB effectively and Eu-In₂O₃ NBs have the potential to be fabricated as H₂S sensors.

Acknowledgments: The authors would like to acknowledge the help of their teachers and friends. This work was supported by the National Natural Science Foundation (Grant No. 11164034), the Key Applied Basic Research Program of Science and Technology Commission Foundation of Yunnan Province (Grant No. 2013FA035), and Innovative talents of Science and Technology Plan Projects of Yunnan Province (Grant No. 2012HA007).

Author Contributions: Yingkai Liu guided the experiments and revised the paper. Weiwu Chen performed the synthesis of nanobelts, the gas sensitive test, and wrote the paper. Zhaojun Qin and Yuemei Wu carried out the characterization. Shuanghui Li and Peng Ai helped with the data analysis.

Conflicts of Interest: The authors declare no conflict of interest.

References

- Xie, P.; Xiong, Q.H.; Fang, Y.; Qing, Q.; Lieber, C.M. Local electrical potential detection of DNA by nanowire-nanopore sensors. *Nat. Nanotechnol.* **2012**, *7*, 119–125. [[CrossRef](#)] [[PubMed](#)]
- Lu, M.L.; Weng, T.M.; Chen, J.Y.; Chen, Y.F. Ultrahigh-gain single SnO₂ nanowire photodetectors made with ferromagnetic nickel electrodes. *NPG Asia Mater.* **2012**. [[CrossRef](#)]
- Liu, X.; Gu, L.L.; Zhang, Q.P.; Wu, J.Y.; Long, Y.Z.; Fan, Z.Y. All-printable band-edge modulated ZnO nanowire photodetectors with ultra-high detectivity. *Nat. Commun.* **2014**, *5*, 4007. [[CrossRef](#)] [[PubMed](#)]
- Lu, L.; Chen, J.; Wang, W. Wide bandgap Zn₂GeO₄ nanowires as photoanode for quantum dot sensitized solar cells. *Appl. Phys. Lett.* **2013**, *103*. [[CrossRef](#)]
- Zhao, C.H.; Huang, B.Y.; Xie, E.Q.; Zhou, J.Y.; Zhang, Z.X. Improving gas-sensing properties of electrospun In₂O₃ nanotubes by Mg acceptor doping. *Sens. Actuators B Chem.* **2015**, *207*, 313–320. [[CrossRef](#)]
- Zou, X.M.; Wang, J.L.; Liu, X.Q.; Wang, C.L.; Jiang, Y.; Wang, Y.; Xiao, X.H.; Johnny, C.H.; Li, J.C.; Jiang, C.Z.; *et al.* Rational Design of Sub-Parts per Million Specific Gas Sensors Array Based on Metal Nanoparticles Decorated Nanowire Enhancement Mode Transistors. *Nano Lett.* **2013**, *13*, 3287–3292. [[CrossRef](#)] [[PubMed](#)]
- Khiabani, P.S.; Hosseinmardi, A.; Marzbanrad, E.; Ghashghaie, S.; Zamani, C.; Keyanpour-Rad, M.; Raissi, B. NO₂ gas sensor fabrication through AC electrophoretic deposition from electrospun In₂O₃ nanoribbons. *Sens. Actuators B Chem.* **2012**, *162*, 102–107. [[CrossRef](#)]
- Kaur, M.; Jain, N.; Sharma, K.; Bhattacharya, S.; Roy, M.; Tyagi, A.K.; Gupta, S.K.; Yakhmi, J.V. Room-temperature H₂S gas sensing at ppb level by single crystal In₂O₃ whiskers. *Sens. Actuators B Chem.* **2008**, *133*, 456–461. [[CrossRef](#)]
- Sun, X.H.; Hao, H.R.; Ji, H.M.; Li, X.L.; Cai, S.; Zheng, C.M. Nanocasting synthesis of In₂O₃ with appropriate mesostructured ordering and enhanced gas-sensing property. *ACS Appl. Mater. Interfaces* **2014**, *6*, 401–409. [[CrossRef](#)] [[PubMed](#)]
- Lai, X.Y.; Wang, D.; Han, N.; Du, J.; Li, J.; Xing, C.J.; Chen, Y.F.; Li, X.T. Ordered arrays of Bead-Chain-like In₂O₃ Nanorods and their enhanced sensing performance for formaldehyde. *Chem. Mater.* **2010**, *22*, 3033–3042. [[CrossRef](#)]
- Singh, N.; Yan, C.Y.; Lee, P.S. Room temperature CO gas sensing using Zn-doped In₂O₃ single nanowire field effect transistors. *Sens. Actuators B Chem.* **2010**, *150*, 19–24. [[CrossRef](#)]
- Singh, N.; Gupta, R.K.; Lee, P.S. Gold-Nanoparticle-Functionalized In₂O₃ Nanowires as CO Gas Sensors with a significant enhancement in response. *ACS Appl. Mater. Interfaces* **2011**, *3*, 2246–2252. [[CrossRef](#)] [[PubMed](#)]
- Choi, S.W.; Katoch, A.; Sun, G.J.; Wu, P.; Kim, S.S. NO₂-sensing performance of SnO₂ microrods by functionalization of Ag nanoparticles. *J. Mater. Chem. C* **2013**, *1*, 2834–2841. [[CrossRef](#)]

14. Wu, Y.M.; Zhang, H.; Liu, Y.K.; Chen, W.W.; Ma, J.; Li, S.H.; Qin, Z.J. Synthesis and Gas Sensing Properties of Single La-Doped SnO₂ Nanobelts. *Sensors* **2015**, *15*, 14230–14240. [[CrossRef](#)] [[PubMed](#)]
15. Bloor, L.G.; Manzi, J.; Binions, R.; Parkin, I.P.; Pugh, D.; Afonja, A.; Blackman, C.S.; Sathasivam, S.; Carmalt, C.J. Tantalum and Titanium doped In₂O₃ Thin Films by Aerosol-Assisted Chemical Vapor Deposition and their Gas Sensing Properties. *Chem. Mater.* **2012**, *24*, 2864–2871. [[CrossRef](#)]
16. Shen, X.; Yan, B. A novel fluorescence probe for sensing organic amine vapors from Eu³⁺ β-diketonate functionalized Bio-MOF-1 hybrid system. *J. Mater. Chem. C* **2015**, *3*, 7038–7044. [[CrossRef](#)]
17. Hao, Z.M.; Yang, G.C.; Song, X.Z.; Zhu, M.; Meng, X.; Zhao, S.; Song, S.; Zhang, H.J. A Europium(III) based Metal-Organic Framework: Bifunctional properties related to sensing and electronic conductivity. *J. Mater. Chem. A* **2013**, *2*, 237–244. [[CrossRef](#)]
18. Yang, H.X.; Wang, S.P.; Yang, Y.Z. Fabrication of metallic ions doped monodispersed porous In₂O₃ nanospheres. *Mater. Lett.* **2013**, *110*, 45–48. [[CrossRef](#)]
19. Ghosh, S.; Das, K.; Sinha, G.; Lahtinen, J.; De, S.K. Bright white light emitting Eu and Tb Co-Doped Monodisperse In₂O₃ nanocrystals. *J. Mater. Chem. C* **2013**, *1*, 5557–5566. [[CrossRef](#)]
20. Li, Z.P.; Fan, Y.J.; Zhan, J.H. In₂O₃ Nanofibers and Nanoribbons: Preparation by Electrospinning and Their Formaldehyde Gas-Sensing Properties. *Eur. J. Inorg. Chem.* **2010**, *2010*, 3348–3353. [[CrossRef](#)]
21. Ma, J.; Liu, Y.K.; Zhang, H.; Ai, P.; Gong, N.L.; Zhang, Y. Synthesis and high sensing properties of a single Pd-doped SnO₂ nanoribbon. *Nanoscale Res. Lett.* **2014**, *9*, 1–10. [[CrossRef](#)] [[PubMed](#)]
22. Hoa, L.T.; Cuong, N.D.; Hoa, T.T.; Khieu, D.Q.; Long, H.T.; Quang, D.T.; Hoa, N.D.; Hieu, N.V. Synthesis, characterization, and comparative gas sensing properties of tin dioxide nanoflowers and porous nanospheres. *Ceram. Int.* **2015**, *41*, 14819–14825. [[CrossRef](#)]
23. Chen, P.C.; Sukcharoenchoke, S.; Ryu, K.; Arco, L.G.D.; Badmaev, A.; Wang, C.; Zhou, C.W. 2,4,6-Trinitrotoluene (TNT) chemical sensing based on Aligned Single-Walled Carbon Nanotubes and ZnO Nanowires. *Adv. Mater.* **2010**, *22*, 1900–1904. [[CrossRef](#)] [[PubMed](#)]
24. Liu, H.; Li, M.; Voznyy, O.; Hu, L.; Fu, Q.Y.; Zhou, D.X.; Xia, Z.; Sargent, E.H.; Tang, J. Physically Flexible, Rapid-Response Gas Sensor based on Colloidal Quantum Dot Solids. *Adv. Mater.* **2014**, *26*, 2718–2724. [[CrossRef](#)] [[PubMed](#)]
25. Dua, V.; Surwade, S.P.; Ammu, S.; Agnihotra, S.R.; Jain, S.; Roberts, K.E.; Park, S.; Ruoff, R.S.; Manohar, S.K. All-Organic Vapor Sensor using Inkjet-Printed reduced graphene oxide. *Angew. Chem. Int. Ed.* **2010**, *49*, 2154–2157. [[CrossRef](#)] [[PubMed](#)]
26. Yang, W.; Wan, P.; Zhou, X.D.; Hu, J.M.; Guan, Y.F.; Feng, L. An additive-free synthesis of In₂O₃ cubes embedded into graphene sheets and their enhanced NO₂ sensing performance at room temperature. *ACS Appl. Mater. Interfaces* **2014**, *6*, 21093–21100. [[CrossRef](#)] [[PubMed](#)]
27. Neri, G.; Bonavita, A.; Micali, G.; Rizzo, G.; Pinna, N.; Niederberger, M.; Ba, J.H. Effect of the chemical composition on the sensing properties of In₂O₃-SnO₂ nanoparticles synthesized by a non-aqueous method. *Sens. Actuators B Chem.* **2008**, *130*, 222–230. [[CrossRef](#)]
28. Li, Y.S.; Xu, J.; Chao, J.F.; Chen, D.; Ouyang, S.X.; Ye, J.H.; Shen, G.Z. High-aspect-ratio single-crystalline porous In₂O₃ nanobelts with enhanced gas sensing properties. *J. Mater. Chem.* **2011**, *21*, 12852–12857. [[CrossRef](#)]
29. Qurashi, A.; El-Maghraby, E.M.; Yamazaki, T.; Kikuta, T. Catalyst supported growth of In₂O₃ nanostructures and their hydrogen gas sensing properties. *Sens. Actuators B Chem.* **2010**, *147*, 48–54. [[CrossRef](#)]
30. Ma, J.; Liu, Y.K.; Zhang, H.; Ai, P.; Gong, N.L.; Wu, Y.M.; Yu, D.P. Room temperature ppb level H₂S detection of a single Sb-doped SnO₂ nanoribbon device. *Sens. Actuators B Chem.* **2015**, *216*, 72–79. [[CrossRef](#)]
31. Zhang, T.; Gu, F.B.; Han, D.M.; Wang, Z.H.; Guo, G.S. Synthesis, characterization and alcohol-sensing properties of rare earth doped In₂O₃ hollow spheres. *Sens. Actuators B Chem.* **2013**, *177*, 1180–1188. [[CrossRef](#)]

